Electrocatalysis

International Edition: DOI: 10.1002/anie.201606327
German Edition: DOI: 10.1002/ange.201606327

Hydrothermal Synthesis of Metal–Polyphenol Coordination Crystals and Their Derived Metal/N-doped Carbon Composites for Oxygen Electrocatalysis

*Jing Wei, Yan Liang, Yaoxin Hu, Biao Kong, Jin Zhang, Qinfen Gu, Yuping Tong, Xianbiao Wang, San Ping Jiang, and Huanting Wang**

Abstract: *Cobalt (or iron)–polyphenol coordination polymers with crystalline frameworks are synthesized for the first time. The crystalline framework is formed by the assembly of metal ions and polyphenol followed by oxidative self-polymerization of the organic ligands (polyphenol) during hydrothermal treatment in alkaline condition. As a result, such coordination crystals are even partly stable in strong acid (such as 2 M HCl). The metal (Co or Fe)-natural abundant polyphenol (tannin) coordination crystals are a renewable source for the fabrication of metal/carbon composites as a nonprecious-metal catalyst, which show high catalytic performance for both oxygen reduction reaction and oxygen evolution reaction. Such excellent performance makes metal–polyphenol coordination crystals an efficient precursor to fabricate low-cost catalysts for the large-scale application of fuel cells and metal–air batteries.*

Metal–organic coordination materials, such as metal–organic frameworks (MOFs) and infinite coordination polymer particles, have attracted increasing interest owing to their highly tailorable metal and organic ligand precursors, diverse structures and morphologies, as well as various applications, including gas adsorption and separation, catalysis, drug delivery, sensing, and energy storage and conversion.[1] These metal–organic coordination materials are generally synthesized using different metal salts and functional organic ligands (such as trimesic acid and imidazole). Tannic acid (TA) is one of naturally abundant polyphenols, which can coordinate with different kinds of metal ions through its catechol groups. As a typical case, the coordination of catechol-based compounds such as dopa and tannic acid and Fe^{3+} has been widely investigated due to their importance in understanding the adhesion mechanism inspired from mussels, as well as the application for pH-triggered drug delivery utilizing the reversibility of metal–catechol coordination bond under different pH values.[2] Furthermore, a multifunctional metal–TA complex can be prepared by assembling different kinds of metal ions with TA on various substrates, which can be used for positron emission tomography, drug delivery, magnetic resonance imaging, and catalysis.[3] However, the metal–natural polyphenol coordination particles, especially with a regular morphology and crystalline framework, have been rarely reported.[4]

Recently, one of the most important applications for metal–organic coordination materials is to convert them into nanoporous metal/carbon composites at high temperature without requiring any auxiliary template, which exhibit excellent performance in electrochemical energy storage and conversion devices, such as supercapacitors, fuel cells, and batteries.[5] For example, zeolitic imidazolate framework-67 (ZIF-67), assembled by cobalt ions and N-rich imidazole ligands, can be converted into Co/N-doped nanoporous carbon composites after carbonization. The resulting carbon composites can be used as the low-cost catalysts for oxygen reduction reaction (ORR) and oxygen evaluation reaction (OER), which are two important reactions for fuel cells, metal–air batteries, and water splitting, and require noble metal-based catalysts such as Pt and RuO_2.[6] The replacement of noble metals with non-precious-metal catalysts (such as Fe,Co-based metal–carbon composites) is highly desirable for the large-scale applications. Note that most of MOF materials are produced from specially synthesized organic ligands (such as imidazole) to realize the regular porous structure, and the large-scale synthesis of carbon by carbonizing such organic ligands may be inviable from the point of view of economy and sustainability. Natural abundant polyphenol such as TA can be easily obtained from plants, and it is a low-cost, nontoxic, and renewable carbon source. However, the metal–polyphenol coordination derived metal–carbon composites have been rarely exploited for the application of sustainable energy storage and conversion.[7]

Herein, a cobalt (or iron)-polyphenol coordination crystal is first synthesized by the assembly of metal ions and polyphenol followed by oxidative self-polymerization of the organic ligands during hydrothermal treatment. The Co (or Fe)-TA coordination crystals are further demonstrated to be a renewable source to prepare Co (or Fe_3C) nanoparticles/N-doped carbon composites by carbonizing the mixture of metal–TA crystal and dicyandiamide followed by acid etching. The Co (or Fe_3C)/N-doped carbon composites show high

[*] Dr. J. Wei, Y. Liang, Y. X. Hu, Dr. B. Kong, Dr. Y. P. Tong, Dr. X. B. Wang, Prof. H. T. Wang
Department of Chemical Engineering, Monash University
Clayton, Victoria 3800 (Australia)
E-mail: huanting.wang@monash.edu
J. Zhang, Prof. S. P. Jiang
Fuels and Energy Technology Institute & Department of Chemical Engineering, Curtin University
Perth, WA 6102 (Australia)
Dr. Q. F. Gu
Australian Synchrotron
Clayton, Victoria 3168 (Australia)
Supporting information and the ORCID identification number(s) for the author(s) of this article can be found under: http://dx.doi.org/10.1002/anie.201606327.

catalytic activity for ORR in both alkaline and acid conditions. Moreover, the Co/N-doped carbon composites also exhibit an excellent performance for OER in alkaline condition.

Each TA ($C_{76}H_{52}O_{46}$) molecular contains 10 catechol groups (Supporting Information, Figure S1). For simplicity, the chemical structure of TA is illustrated for the ligand with two catechol groups (Figure 1 a). The synthesis of Co-TA

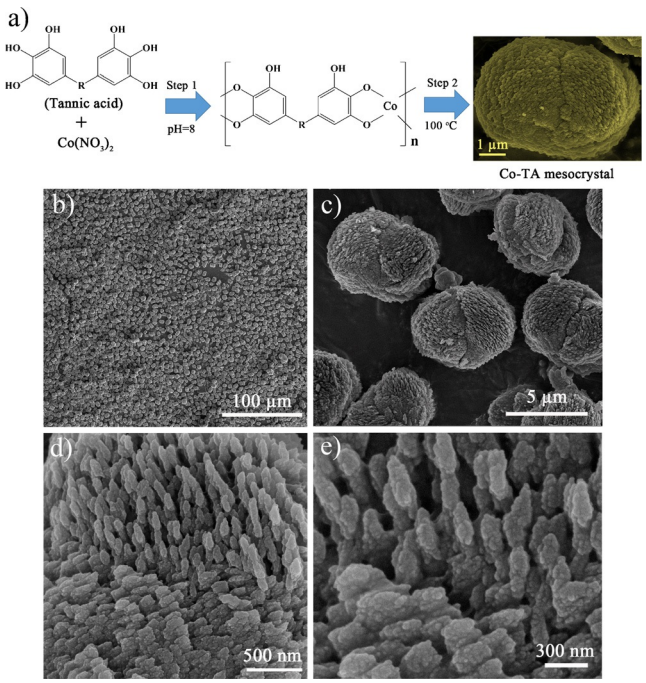

Figure 1. a) Representation of the synthesis of Co-TA crystals. Step 1: self-assembly of Co ions and tannic acid in alkaline aqueous solution to form Co-TA complex; Step 2: hydrothermal treatment of Co-TA complex to synthesize Co-TA crystals. b)–e) SEM images of Co-TA crystals.

coordination crystals includes two steps. First, the Co-TA coordination structure is formed by the self-assembly of cobalt ions and TA in alkaline condition. The pH value of TA aqueous solution (12.5 mg mL^{-1}) before adding the cobalt precursor is about 3. In such acidic conditions, one cobalt ion may only coordinate with one catechol group, resulting in a clear solution with soluble Co-TA complex (Supporting Information, Figure S2a). By comparison, the pH value of TA solution increases to 8 after adding ammonium hydroxide. The catechol groups can be deprotonated and chelate with Co ion strongly. In this case, one cobalt ion can coordinate with two catechol groups from different TA molecules, resulting in the coordination polymerization (Supporting Information, Figure S2a). The resulting precipitates exhibit an irregular morphology and amorphous structure (Supporting Information, Figure S3), indicating that the direct self-assembly of Co^{2+} and TA in alkaline aqueous solution does not produce the Co-TA crystals.

In the second step, the crystalline framework is formed by a further hydrothermal treatment. Scanning electron microscopy (SEM) images of Co-TA crystals reveal the uniform particles with a size of around 5 μm (Figure 1 b). These particles are assembled by spindle-like subunits (Figure 1 c). Interestingly, these spindle-like subunits are composed of smaller nanoparticles (Figure 1 d,e). Transmission electron microscopy (TEM) images and corresponding element mapping of Co-TA crystals reveal that these spindle-like subunits are composed of carbon, oxygen, and cobalt elements (Supporting Information, Figure S4). X-ray photoelectron spectroscopy (XPS) spectra of Co-TA coordination crystals also reveal the main compositions are carbon, oxygen, and cobalt (Supporting Information, Figure S5). The high-resolution Co 2p XPS spectra reveals the formation of Co^{II}–O bonds (Supporting Information, Figure S5c).[8] X-ray diffraction (XRD) patterns of Co-TA obtained after hydrothermal treatment reveal a highly crystalline framework, which is different from that of Co_3O_4 crystals prepared using the same method without adding TA (Figure 2 a; Supporting Information, Figure S6). The synchrotron X-ray powder diffraction of

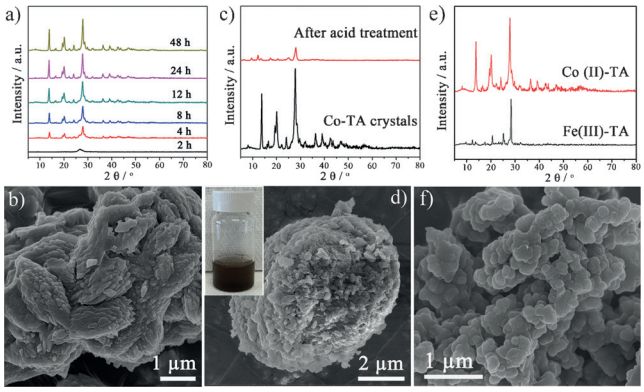

Figure 2. XRD patterns of a) Co-TA complex obtained with different hydrothermal times (2–48 h); c) Co-TA-12 before and after acid treatment and e) Fe^{III}-TA and Co^{II}-TA crystals. SEM images of b) Co-TA-4, d) Co-TA crystal after treatment with acid and f) Fe-TA crystals. Inset in (d): a Co-TA crystal dispersed in 2 M HCl.

Co-TA coordination crystals further prove the highly crystalline framework (Supporting Information, Figure S7). Although it is unlikely to determine the exact crystal structure based on the existing results, it is confirmed that new cobalt–TA coordination crystals are definitely obtained. According to Bergström and Cölfen's definition,[9] the cobalt–TA coordination crystals can be defined as metal–organic coordination mesocrystals. It is worth mentioning that most of reported mesocrystals are inorganic crystals, such as metal oxide and carbonate.[9] As far as we know, cobalt–TA coordination crystals are the first example of metal–TA coordination mesocrystals reported to date.

To investigate the possible formation process of Co–TA coordination crystals, the Co–TA complex was treated under hydrothermal conditions at different times. The resulting samples were denoted Co-TA-*x* (*x* refers to the time of hydrothermal treatment, $x = 2$–48 h). Co-TA-2 exhibits amorphous structure and irregular morphology (Figure 2 a; Supporting Information, Figure S8). After 4 h of hydrothermal treatment (Co-TA-4), the spindle-like Co-TA complex with crystalline framework appears, implying the beginning of crystallization process (Figure 2 a,b). Upon extending the hydrothermal time further up to 48 h, the crystalline structure

of the Co–TA coordination structure (Co-TA-48) does not change obviously. However, SEM images show these spindle-like subunits can assemble to different morphologies, indicating Co–TA coordination structure is not stable under hydrothermal treatment and undergoes further recrystallization. The resulting Co-TA crystals show the similar microstructure upon changing the ratio of Co source and TA (Supporting Information, Figure S9).

Based on the above results, we propose that the formation mechanism of Co–TA crystals is driven by the self-assembly of cobalt ion and TA via coordination interactions followed by oxidative self-polymerization of organic ligands during hydrothermal treatment. The base can deprotonate the dihydroxy groups of catechol moieties, resulting in a stronger chelating ability with metal ions. At the same time, the catechol groups can be oxidized to quinone by the dissolved oxygen in alkaline solution. Then, the radical generation and oxidative coupling process of catechol occur, resulting in oxidation polymerization.[10] In our experimental condition, the chelating and oxidation processes occur simultaneously. However, their reaction rates are different. In the first step, the precipitate of Co–TA complex can be dissolved completely after adding 2 M HCl (Supporting Information, Figure S2), indicating that the precipitate is mainly formed via the coordination reaction of metal ions and catechol groups. The proton dissociated from the acid can replace the cobalt ions to disassemble the Co-TA coordination, resulting in the dissolution of the Co-TA coordination structure. The color of the supernatant with aqueous ammonia changes from pink to brown, implying that the TA molecules are oxidized by dissolved oxygen to produce oligomers. After hydrothermal treatment, the precipitate of coordinated Co-TA cannot be fully dissolved in acid (Figure 2c,d). An SEM image of Co–TA coordination crystals after treating with 2 M HCl reveals that the particle morphology does not change much but the spindle-like subunits are partially degraded. The crystalline framework is still partly preserved as shown in XRD patterns. These results confirm the oxidative polymerization of TA ligand occurs during the hydrothermal treatment. As a result, the Co–TA coordination crystals are more stable in acidic condition than Co–TA complex without hydrothermal treatment. During the hydrothermal process, the crystalline framework is formed, driven by the rearrangement and recrystallization of the metal and ligands. Furthermore, Fe^{III}–TA coordination crystals could be also synthesized by the same process, indicating this method is versatile for synthesis of metal–TA crystals (Figure 2e,f).

Cobalt-based metal–organic framework-derived carbon composites could be used as a bifunctional catalyst for both ORR and OER, which is a promising substitution of noble metal catalysts.[11] As a proof-of-concept, the Co-TA crystals were also used as carbon and cobalt sources (Figure 3a). Thermogravimetric results confirm the feasibility of conversion of Co-TA into a cobalt–carbon composite, and SEM images reveal that the morphology and microstructure for the resulting cobalt/carbon composites are partially retained (Supporting Information, Figure S10). Doping of nitrogen atoms in the carbon is desirable as it can form active sites for ORR such as pyridinic-nitrogen/C and Co-N_x/C.[12] In our

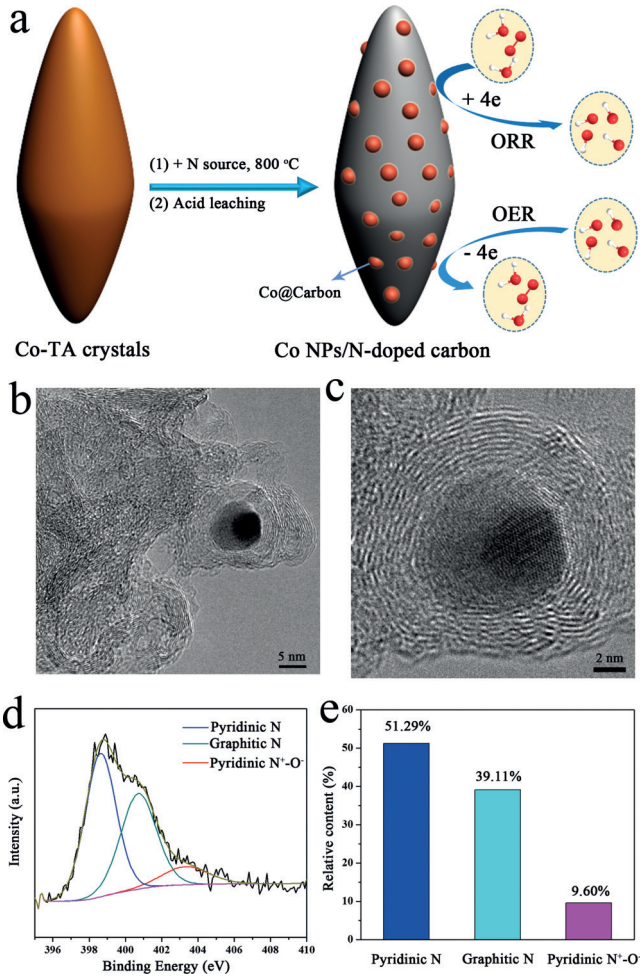

Figure 3. a) Illustration of the preparation of Co nanoparticles embedded in the N-doped carbon as bifunctional electrocatalysts for ORR and OER in alkaline conditions. b), c) TEM images of Co-TA-800. d), e) XPS N 1s spectra for Co-TA-800 and the relative content of N element with different bonding configurations.

experiments, dicyandiamide with a high nitrogen content of 67 wt % was chosen as a nitrogen source. Co-TA crystals were ground with dicyandiamide, followed by carbonization at 800 °C and acid leaching, Co nanoparticles/N-doped carbon composites were obtained and denoted Co-TA-800.

TEM and XRD results of Co-TA-800 reveal that cobalt nanoparticles are dispersed in the carbon matrix (Supporting Information, Figure S11, S12). The corresponding element mapping images show that the nitrogen is distributed in the carbon matrix uniformly, indicating successful nitrogen doping. High-magnification TEM images show the cobalt nanoparticles are encapsulated by a few layers of graphitized carbon to form a core–shell Co@C structure (Figure 3b,c). XPS peaks for the N 1s, which can be fitted with three peaks at about 398.63, 400.71, and 403.31 eV, are assigned to pyridinic nitrogen, graphitic nitrogen, and pyridinic N^+–O^- (Figure 3d,e, Supporting Information, Figure S13). Their relative contents are 51.29, 39.11, and 9.60 % respectively. The high content of pyridinic nitrogen is required because the pyridinic nitrogen more likely forms the active sites.[12] In the high resolution spectrum of the Co 2p region, the peaks with

binding energy of 780.12 and 781.73 eV could be attributed to oxygen- and nitrogen-coordinated Co, respectively, implying the formation of Co–O and Co–N_x structure.[6] The BET surface area for Co-TA-800 is 180 $m^2 g^{-1}$ from the N_2 sorption measurement (Supporting Information, Figure S14).

The ORR performance of Co-TA derived catalysts was evaluated using a rotating disk electrode technique. Cyclic voltammetry curves reveal a clear oxygen reduction peak for all the materials, implying an oxygen reduction activity (Supporting Information, Figure S15). The linear scan voltammogram (LSV) curves for Pt/C and Co-TA-x ($x = 700$, 800, 900) at a rotating speed of 1600 rpm in O_2-saturated 0.1 M KOH solution show their onset potential are at 0.94, 0.85, 0.95, and 0.91 V (versus reversible hydrogen electrode, vs. RHE), respectively (Figure 4a). Co-TA-800 has slightly

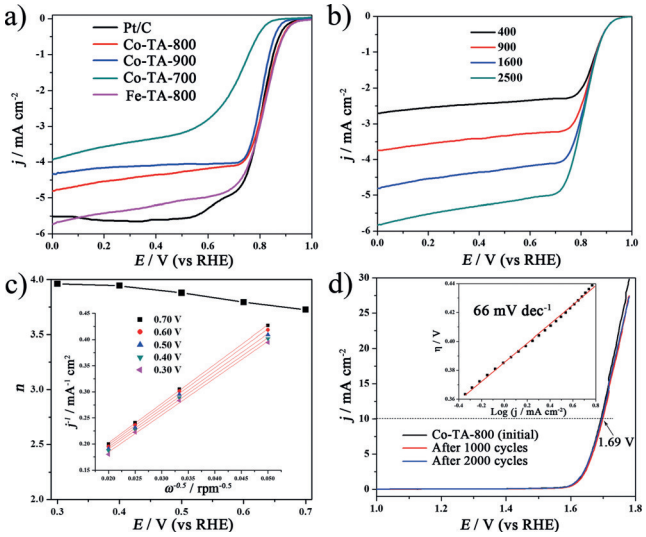

Figure 4. a) Linear scan voltammogram (LSV) of commercial Pt/C, Co-TA-700, Co-TA-800, Co-TA-900 and Fe-TA-800 for ORR; b) LSV curves of Co-TA-800 recorded with different rotating speeds; c) electron transfer numbers and corresponding K-L plots (inset) of Co-TA-800; d) LSV curves and corresponding Tafel plots (inset) of Co-TA-800 for OER.

higher onset potential than commercial Pt/C (20 wt%, Sigma–Aldrich, Australia), implying a higher catalytic activity. The corresponding limiting current density at 0.30 V are 5.6, 3.4, 4.4, and 4.1 mA cm^{-2}, respectively. Co-TA-800 exhibits better performance than Co-TA-700 and Co-TA-900 owing to the optimized compositions and conductivity (Supporting Information, Figure S15e,f). Furthermore, Co-TA-800 shows better performance than that derived from amorphous Co-TA complex (Supporting Information, Figure S16), indicating the crystalline framework is beneficial for the improvement of catalytic activity. The Koutechy–Levich (K-L) plots of Co-TA-800 calculated from LSV curves at different rotating speeds exhibit a good linearity with the similar slop (Figure 4b,c), indicating a first-order reaction and similar electron transfer numbers (n). The n value for Co-TA-800 is 3.7–4.0, implying a near-four-electron pathway. Co-TA-800 also has better long-term stability and higher resistance to the methanol cross-over effect than Pt/C. The ORR performance of Co-TA-800 in acidic condition was also investigated (Supporting Information, Figure S17) and Co-TA-800 is among the best of non-precious metal catalyst reported to date (Supporting Information, Table S1, S2).

Apart from the Co-TA, Fe-TA coordination crystals were also used as a precursor, and their derived iron carbide/carbon (denoted Fe-TA-800) show higher ORR catalytic activity than Co-TA-800 in both alkaline and acid conditions (Figure 4a; Supporting Information, Figures S12, S14, S18–S20, Table S1, S2). The long-term stability for Fe-TA-800 is slightly lower than that of Co-TA-800. These results further confirm the metal–TA crystals are the excellent precursors for the synthesis of metal (or metal carbide)/carbon composites with high catalytic performance. The Fe (or Co)-N_x-C has been considered as the efficient catalytic active site for ORR. The metal (Co) or metal carbide (Fe_3C) nanoparticles encapsulated by graphitic carbon layer could also improve the catalytic performance of the neighboring carbon owing to the strong electronic interactions between the metal and neighboring carbon.[13] Recently, Jiang et al. demonstrated the Fe_3C nanoparticles encapsulated by carbon could boost the activity of Fe-N_x-C.[14] Herein, the high catalytic activity could be attributed to the coexistence of metal-N_x-C and cobalt (or iron carbide) nanoparticles and their synergetic catalytic effect in enhancing the catalytic performance.

The OER performance of Co-TA-800 was also preliminarily evaluated in O_2-saturated 0.1 M KOH solution (Figure 4d). LSV curves of Co-TA-800 show the potential is 1.69 V vs. RHE at the current density of 10 mA cm^{-2} (based on geometric electrode area), which is comparable to other recently reported bifunctional oxygen catalysts (Supporting Information, Table S3). Tafel plots for Co-TA-800 reveal a low slope of 66 mV $decade^{-1}$, indicating a favorable reaction kinetics. After 1000 and 2000 continuous cycles, the potentials at the current density of 10 mA cm^{-2} are not changed obviously, indicating a high stability. Such results further prove metal–TA crystals are also a good precursor for the fabrication of efficient catalysts in the applications of metal-air batteries and water splitting.

In summary, metal–polyphenol coordination crystals are synthesized via the assembly of metal ions and tannic acid, followed by the oxidative self-polymerization of organic ligands under hydrothermal treatment. The obtained crystals show uniform structure and are stable in acid. Such metal (Co, Fe)–TA crystals can be used as the low-cost and renewable source to fabricate cobalt (or Fe_3C) nanoparticles/N-doped carbon composites, which show high catalytic performance for both ORR and OER. This synthesis route opens an avenue for the preparation of various kinds of metal-polyphenol coordination with crystalline framework and acid-resistance, such as Ni-TA, Cu-TA, Zn-TA, and Ti-TA. These metal–organic frameworks could be useful for adsorption, catalysis, and biomedicine. Furthermore, such metal–polyphenol crystals can also be used as the sustainable source to fabricate metal (or metal carbide)/carbon composites after controllable carbonization, which would be applied as useful electrode materials for sustainable energy conversion and storage.

Acknowledgements

This work is supported by the Australian Research Council through Discovery grants (Project No. DP150100765, DP150102044). The XRPD experiment was performed at PD beamline, Australian Synchrotron. We thank Jean-Pirerre Veder of Curtin University and Xi-Ya Fang of Monash Center for Electron Microscopy for their assistance with the XPS and SEM characterization, respectively. The authors acknowledge the use of equipment, scientific and technical assistance of the WA X-Ray Surface Analysis Facility, funded by the Australian Research Council LIEF grant LE120100026.

Keywords: cobalt · metal–tannin framework · nonprecious-metal catalysts · oxygen reduction reaction · polyphenol

How to cite: *Angew. Chem. Int. Ed.* **2016**, *55*, 12470–12474
Angew. Chem. **2016**, *128*, 12658–12662

[1] a) H. Li, M. Eddaoudi, M. O'Keeffe, O. M. Yaghi, *Nature* **1999**, *402*, 276; b) J. S. Seo, D. Whang, H. Lee, S. I. Jun, J. Oh, Y. J. Jeon, K. Kim, *Nature* **2000**, *404*, 982; c) S. Kitagawa, R. Kitaura, S. Noro, *Angew. Chem. Int. Ed.* **2004**, *43*, 2334; *Angew. Chem.* **2004**, *116*, 2388; d) J. Lee, O. K. Farha, J. Roberts, K. A. Scheidt, S. T. Nguyen, J. T. Hupp, *Chem. Soc. Rev.* **2009**, *38*, 1450; e) J.-R. Li, R. J. Kuppler, H.-C. Zhou, *Chem. Soc. Rev.* **2009**, *38*, 1477; f) J. R. Long, O. M. Yaghi, *Chem. Soc. Rev.* **2009**, *38*, 1213; g) A. M. Spokoyny, D. Kim, A. Sumrein, C. A. Mirkin, *Chem. Soc. Rev.* **2009**, *38*, 1218; h) L. E. Kreno, K. Leong, O. K. Farha, M. Allendorf, R. P. Van Duyne, J. T. Hupp, *Chem. Rev.* **2012**, *112*, 1105; i) Q.-L. Zhu, Q. Xu, *Chem. Soc. Rev.* **2014**, *43*, 5468.

[2] a) H. Lee, S. M. Dellatore, W. M. Miller, P. B. Messersmith, *Science* **2007**, *318*, 426; b) M. J. Harrington, A. Masic, N. Holten-Andersen, J. H. Waite, P. Fratzl, *Science* **2010**, *328*, 216; c) H. Ejima, J. J. Richardson, K. Liang, J. P. Best, M. P. van Koeverden, G. K. Such, J. Cui, F. Caruso, *Science* **2013**, *341*, 154.

[3] J. Guo, Y. Ping, H. Ejima, K. Alt, M. Meissner, J. J. Richardson, Y. Yan, K. Peter, D. von Elverfeldt, C. E. Hagemeyer, *Angew. Chem. Int. Ed.* **2014**, *53*, 5546; *Angew. Chem.* **2014**, *126*, 5652.

[4] a) N. T. Nguyen, H. Furukawa, F. Gándara, C. A. Trickett, H. M. Jeong, K. E. Cordova, O. M. Yaghi, *J. Am. Chem. Soc.* **2015**, *137*, 15394; b) S. J. Yang, M. Antonietti, N. Fechler, *J. Am. Chem. Soc.* **2015**, *137*, 8269; c) P. Zhang, H. Li, G. M. Veith, S. Dai, *Adv. Mater.* **2015**, *27*, 234.

[5] a) B. Liu, H. Shioyama, T. Akita, Q. Xu, *J. Am. Chem. Soc.* **2008**, *130*, 5390; b) W. Xia, A. Mahmood, R. Zou, Q. Xu, *Energy Environ. Sci.* **2015**, *8*, 1837.

[6] a) X. Wang, J. Zhou, H. Fu, W. Li, X. Fan, G. Xin, J. Zheng, X. Li, *J. Mater. Chem. A* **2014**, *2*, 14064; b) W. Xia, J. Zhu, W. Guo, L. An, D. Xia, R. Zou, *J. Mater. Chem. A* **2014**, *2*, 11606; c) Y. Hou, Z. Wen, S. Cui, S. Ci, S. Mao, J. Chen, *Adv. Funct. Mater.* **2015**, *25*, 872; d) J. Wei, Y. Hu, Y. Liang, B. Kong, J. Zhang, J. Song, Q. Bao, G. P. Simon, S. P. Jiang, H. Wang, *Adv. Funct. Mater.* **2015**, *25*, 5768; e) J. Wei, Y. Hu, Z. Wu, Y. Liang, S. Leong, B. Kong, X. Zhang, D. Zhao, G. P. Simon, H. Wang, *J. Mater. Chem. A* **2015**, *3*, 16867; f) A. Aijaz, J. Masa, C. Rösler, W. Xia, P. Weide, A. J. Botz, R. A. Fischer, W. Schuhmann, M. Muhler, *Angew. Chem. Int. Ed.* **2016**, *55*, 4087; *Angew. Chem.* **2016**, *128*, 4155; g) Z. Li, M. Shao, L. Zhou, R. Zhang, C. Zhang, M. Wei, D. G. Evans, X. Duan, *Adv. Mater.* **2016**, *28*, 2337; h) Y. Z. Chen, C. Wang, Z. Y. Wu, Y. Xiong, Q. Xu, S. H. Yu, H. L. Jiang, *Adv. Mater.* **2015**, *27*, 5010; i) A. Mahmood, W. H. Guo, H. Tabassum, R. Q. Zou, *Adv. Energy. Mater.* **2016**, 1600423; j) S. J. You, X. B. Gong, W. Wang, D. P. Qi, X. H. Wang, X. D. Chen, N. Q. Ren, *Adv. Energy Mater.* **2016**, *6*, 1501497; k) L. Xu, Q. Jiang, Z. Xiao, X. Li, J. Huo, S. Wang, L. Dai, *Angew. Chem. Int. Ed.* **2016**, *55*, 5277; *Angew. Chem.* **2016**, *128*, 5363; l) S. Dou, L. Tao, J. Huo, S. Wang, L. Dai, *Energy Environ. Sci.* **2016**, *9*, 1320.

[7] J. Wei, Y. Liang, Y. Hu, B. Kong, G. P. Simon, J. Zhang, S. P. Jiang, H. Wang, *Angew. Chem. Int. Ed.* **2016**, *55*, 1355; *Angew. Chem.* **2016**, *128*, 1377.

[8] a) X. Wang, L. Lu, Z. Yu, X. Xu, Y. Zheng, S. Yu, *Angew. Chem. Int. Ed.* **2015**, *54*, 2397; *Angew. Chem.* **2015**, *127*, 2427; b) Z. Yu, Z. Wu, S. Xin, C. Qiao, Z. Yu, H. Cong, S. Yu, *Chem. Mater.* **2014**, *26*, 6915.

[9] L. Bergström, E. V. Sturm, G. Salazar-Alvarez, H. Cölfen, *Acc. Chem. Res.* **2015**, *48*, 1391.

[10] a) M. Yu, J. Hwang, T. J. Deming, *J. Am. Chem. Soc.* **1999**, *121*, 5825; b) L. A. Burzio, J. H. Waite, *Biochemistry* **2000**, *39*, 11147; c) Y. Liu, K. Ai, L. Lu, *Chem. Rev.* **2014**, *114*, 5057; d) T. S. Sileika, D. G. Barrett, R. Zhang, K. H. A. Lau, P. B. Messersmith, *Angew. Chem. Int. Ed.* **2013**, *52*, 10766; *Angew. Chem.* **2013**, *125*, 10966; e) H. Xu, J. Nishida, W. Ma, H. Wu, M. Kobayashi, H. Otsuka, A. Takahara, *ACS Macro Lett.* **2012**, *1*, 457.

[11] T. Y. Ma, S. Dai, M. Jaroniec, S. Z. Qiao, *J. Am. Chem. Soc.* **2014**, *136*, 13925.

[12] a) K. Gong, F. Du, Z. Xia, M. Durstock, L. Dai, *Science* **2009**, *323*, 760; b) M. Lefèvre, E. Proietti, F. Jaouen, J.-P. Dodelet, *Science* **2009**, *324*, 71; c) G. Wu, K. L. More, C. M. Johnston, P. Zelenay, *Science* **2011**, *332*, 443; d) D. Guo, R. Shibuya, C. Akiba, S. Saji, T. Kondo, J. Nakamura, *Science* **2016**, *351*, 361.

[13] D. Deng, L. Yu, X. Chen, G. Wang, L. Jin, X. Pan, J. Deng, G. Sun, X. Bao, *Angew. Chem. Int. Ed.* **2013**, *52*, 371; *Angew. Chem.* **2013**, *125*, 389.

[14] W. J. Jiang, L. Gu, L. Li, Y. Zhang, X. Zhang, L. J. Zhang, J. Q. Wang, J. S. Hu, Z. Wei, L. J. Wan, *J. Am. Chem. Soc.* **2016**, *138*, 3570.

Received: June 29, 2016
Published online: September 1, 2016

